Academic Journal of Science and Technology
ISSN: 2771-3032 | Vol. 23, No. 3, 2026

Research on Trajectory Planning of Carbide Discharge Robotic Arm Based on Inverse Kinematics

Kehan Peng, Dazhi Yang*

Sichuan University of Science and Engineering, Yibin Sichuan 644000, China
* Corresponding author

Abstract: In response to the harsh working environment of carbide furnaces, which is characterized by high temperatures, intense light, high dust levels, and high risks, this paper proposes a trajectory planning method for the end effector of a carbide discharge robot based on inverse kinematics. This method achieves remote control of the ablation trajectory of the robotic arm by establishing a model of the arm and deriving inverse kinematic joint pose equations. The paper elaborates on the complete control process of the robotic arm performing ablation operations at the furnace mouth. Simulation verification of the robotic arm's workspace and ablation trajectories for horn-shaped and cylindrical furnace mouths is conducted on the MATLAB platform, enabling it to efficiently burn through the carbide furnace at predetermined points, thereby effectively avoiding safety hazards for personnel exposed to dangerous environments. The results show that this trajectory planning method enables the robotic arm to complete the burn-through operation of a 600 mm thickness within 180 seconds, with high control accuracy and response speed. It can stably achieve automated discharge operations under remote control, significantly improving the intrinsic safety level and operational reliability of the production process.

Keywords: Inverse kinematics; tapping robotic arm; trajectory planning; remote control; MATLAB simulation.

1. Introduction

Currently, China's calcium carbide industry is in a period of transformation and upgrading. Although its annual production capacity remains stable at around 42 million tons, the issue of low operating rates remains prominent. As a basic chemical raw material, the improvement of its production environment is urgent. The introduction of industrial robotic arms provides an opportunity to address this challenge. This technology is known for its high precision, reliability, and speed[1], making it particularly suitable for replacing manual labor in high-risk and harsh environments. In the calcium carbide furnace tapping process, manual teaching relies on experience-based operations and lacks global optimization thinking. Path confusion is prone to occur in complex areas, resulting in low slag removal efficiency and insufficient operational efficiency, making it difficult to meet the needs of large-scale industrial production[2]. Therefore, relying on robotic arm technology to develop a dedicated tapping trajectory planning algorithm is not only a key measure to break production constraints but also an inevitable choice for achieving the coordinated development of intrinsic safety and quality improvement.

The mechanical arm for calcium carbide discharge adopts a hybrid configuration of "track + RRP", featuring freedom of movement on the track and equipped with rotating, pitching, and linear telescopic joints on the upper part. In the control of the mechanical arm, the inverse kinematics (IK) algorithm is crucial for precise pose control of the end effector, achieving a predetermined trajectory by solving the real-time angles of each joint. However, the working conditions of calcium carbide discharge are extremely special and the environment is dynamically complex, posing stringent requirements for path accuracy and efficiency[3]. The mechanical arm must not only ensure high-precision position tracking but also possess strong environmental adaptability, which places higher demands on the robustness and solving efficiency of the inverse kinematics algorithm.

In the literature[4], a PLC-based tapping control system was designed, and basic motion tests were conducted on the actuator, initially achieving remote control. In the literature[5], based on the research of motor control algorithms, a tapping robotic arm pose adjustment control system and its overall structure were designed. Meanwhile, reasonable hardware selection was made, and the electrical connection and control cabinet design and debugging were completed, ensuring the system achieved good accuracy indicators. In the literature [6], the monitoring system at the tapping site was modified to address the hazards of strong light and high heat to human health. In the literature[7], focusing on various trajectory planning schemes, the pose response characteristics of each joint of the robotic arm were studied, thereby enhancing the smoothness of system operation. In the literature[8], SUN et al. reviewed the research progress on Cartesian space feed rate and joint space trajectory planning in robotic arm machining. In the literature [9], WANG et al. proposed a constant feed rate scheduling strategy, which effectively ensured the smoothness of the machining process, suppressed vibration, and protected the end effector; experimental verification showed that this method could achieve higher workpiece surface quality. In the literature[10], facing the working conditions of the outlet of a shaft furnace, Pietro et al. developed a new type of eye-opening and blocking machine by integrating the functions of an opening machine and a clay gun, successfully realizing the mechanization of tapping operations for ferroalloys and metallic iron ore. In the literature[11], Zhao Jing et al. used the angle, angular velocity, and angular acceleration of the robotic arm joints as constraints, generated trajectories using a fifth-order polynomial interpolation method in joint space, and established an optimization model aimed at reducing operation time, achieving good results.

Facing the precise operation requirements of the carbide tapping robotic arm in complex environments, this paper

proposes an efficient and stable inverse kinematics solving method, and constructs a horn-shaped and cylindrical trajectory planning control system. Addressing the current situation of low automation in carbide furnace port ablation, the study deeply analyzes the characteristics of the tapping process and combines the robotic arm dynamics model to systematically study the inverse kinematics algorithm and trajectory control strategy. Experimental verification shows that this strategy significantly improves the operation efficiency and safety of the robotic arm, providing reliable technical support for the development of carbide tapping automation.

2. Introduction to the Discharge Robotic Arm

The discharging robotic arm is mainly composed of a rail car, a base, a large arm, a small arm, and an extendable arm, as shown in Figure 1.

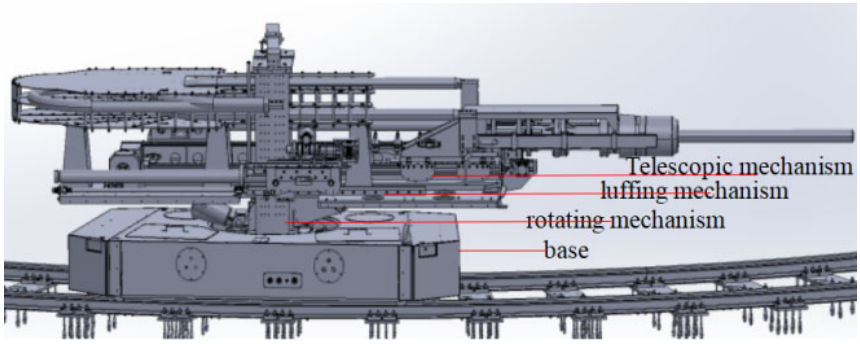


Figure 1. Discharge robotic arm

The robotic arm possesses three degrees of freedom, namely the rotational joint, pitch joint, and telescopic joint, which are simplified as shown in Figure 2.

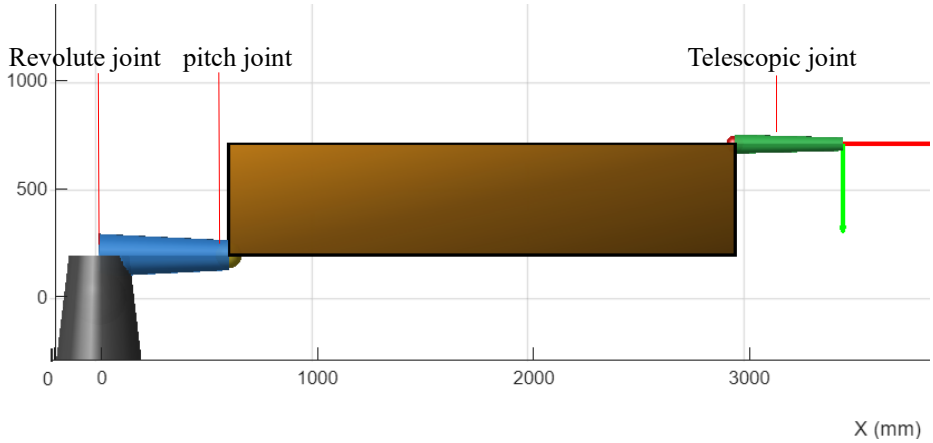


Figure 2. Outlet Mechanical Arm Diagram Section

Currently, the carbide tapping process consists of furnace hole maintenance, furnace opening, and hole blocking, etc. Most enterprises still adopt traditional manual operations for tapping, with the operational steps shown in Figure 3.

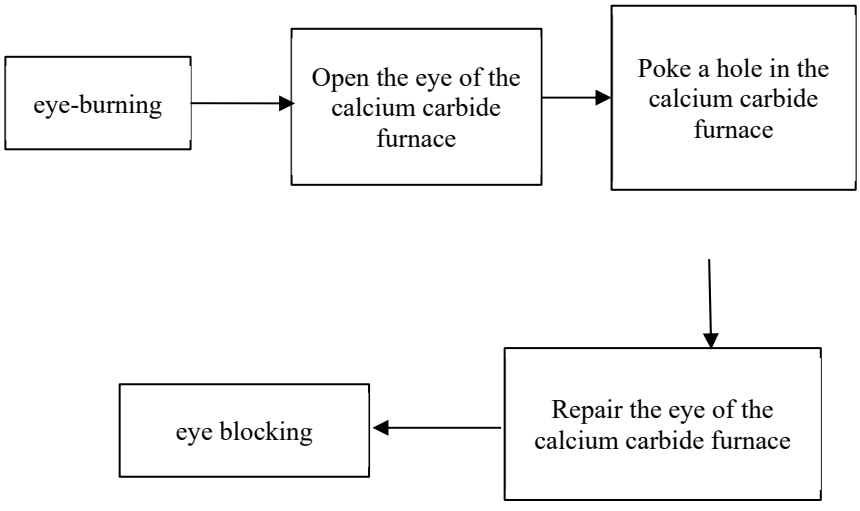


Figure 3. Discharge process

3. Kinematics Modeling of The Discharge Robotic Arm

3.1. Establishment of D-H coordinate system for robotic arm

Utilizing the D-H (Denavit-Hartenberg) parameter method[12] and incorporating the simplified diagram of the robotic arm joints depicted in Figure 2, one can construct a motion model and coordinate system schematic for the industrial robotic arm[13] (refer to Figure 4).

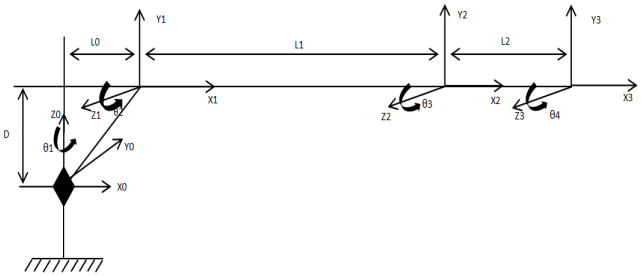


Figure 4. Simplified diagram of robotic arm joints

Furthermore, given that the initial joint rotation angles θ_1 and θ_2 of the three-degree-of-freedom industrial robotic arm directly correspond to the joint angles, and all other parameters are constants, its D-H parameter table can be constructed based on the simplified diagram of the link coordinate system (see Table 1 for details). Based on this model, only the first two joint variables are required to determine the end-effector pose of the burn-through device of the furnace robotic arm[14]. Table1 presents the D-H parameter table for the furnace robotic arm.

Table 1. D-H parameter table of the tapping machine arm

Joint	Linkage torsion angle α_i	Connecting rod length a_i	Connecting rod offset d_i	Joint angle θ_i
1	α_1	l_1	d_1	θ_1
2	0	l_2	0	θ_2
3	0	0	d_3	0

In Table 1, α_1=-90°, l_1=600mm, l_2=2345mm, d_1=196mm, and d_3=0~2000mm. The relationship between the end position of the robotic arm and the base coordinate system is as follows:

$$ {}^0_3T = \prod_{i=3}^{3} {}^{i-1}_{i}T = {}^0_1T\ {}^1_2T\ {}^2_3T \tag{1} $$

In the formula, ${}^{i-1}_{i}T$ represents the rotation transformation matrix of the i-th link relative to the i-1-th link. The formula for the transformation matrix of adjacent links is as follows[14]:

$$ A_1 = \begin{bmatrix} \cos\theta_1 & 0 & -\sin\theta_1 & 600\cos\theta_1 \\ \sin\theta_1 & 0 & \cos\theta_1 & 600\sin\theta_1 \\ 0 & -1 & 0 & 196 \\ 0 & 0 & 0 & 1 \end{bmatrix} \tag{2} $$

$$ A_2 = \begin{bmatrix} \cos\theta_2 & -\sin\theta_2 & 0 & 2345\cos\theta_2 \\ \sin\theta_2 & \cos\theta_2 & 0 & 2345\sin\theta_2 \\ 0 & 0 & 1 & 0 \\ 0 & 0 & 0 & 1 \end{bmatrix} \tag{3} $$

$$ A_3 = \begin{bmatrix} 1 & 0 & 0 & 0 \\ 0 & 1 & 0 & 0 \\ 0 & 0 & 1 & d_3 \\ 0 & 0 & 0 & 1 \end{bmatrix} \tag{4} $$

The following is the end-effector pose matrix obtained by multiplying the three local matrices $A_1A_2A_3$ mentioned above. It describes the absolute position and orientation of the end-effector relative to the base, incorporating the influence of all joint variables:

$$ T = \begin{bmatrix} \cos\theta1\cos\theta2 & -\cos\theta1\sin\theta2 & -\sin\theta1 & \cos\theta1(600+2345\cos\theta2+d3\sin\theta2) \\ \sin\theta1\cos\theta2 & -\sin\theta1\sin\theta2 & \cos\theta1 & \sin\theta1(600+2345\cos\theta2+d3\sin\theta2) \\ -\sin\theta2 & -\cos\theta2 & 0 & 196-2345\sin\theta2+d3\cos\theta2 \\ 0 & 0 & 0 & 1 \end{bmatrix} $$

$$ = \begin{bmatrix} n_x & o_x & a_x & p_x \\ n_y & o_y & a_y & p_y \\ n_z & o_z & a_z & p_z \\ 0 & 0 & 0 & 1 \end{bmatrix} \tag{5} $$

As the core cornerstone of robotic arm trajectory planning and motion control, inverse kinematics solving is not only more complex than forward kinematics, but also often characterized by multi-solution or no solution. The paper adopts an algebraic method to derive the inverse solution for the robotic arm. Given that the third joint is a prismatic pair, the analytical expressions for the angles of the first two rotational joints are obtained through calculation as follows:

$$ \theta_1 = a\tan 2\left(P_y, P_x\right) \tag{6} $$

$$ r' = \sqrt{P_x^2 + P_y^2} - 600 \tag{7} $$

$$ z' = P_z - 196 \tag{8} $$

$$ d_3 = \sqrt{r'^2 + z'^2 - 2345^2} \tag{9} $$

$$\theta_2 = a\tan 2\left(d_3 \cdot r' - 2345 \cdot z', 2345 \cdot r' + d_3 \cdot z'\right) \quad (10)$$

4. Kinematics Analysis of Robotic Arm

4.1. Kinematics verification of robotic arm

To verify the correctness of the forward kinematics model of the robotic arm, the rotation angle θ and extension d of each joint axis can be given, and the results can be obtained through robot toolbox simulation and theoretical formula calculation, respectively. If the outputs of the two methods are consistent, it indicates that the derived forward kinematics solution method is accurate and reliable[14].

Set the joint parameters of each robotic arm as θ_1=30°, θ_2=45°, and d_3=500, and substitute them into the theoretical formula for solution; simultaneously, call the forward kinematics function fkine in the robot toolbox to perform forward kinematics calculations. The resulting pose matrix is as follows:

$$T = \begin{bmatrix} 0.61 & -0.61 & -0.50 & 2261.73 \\ 0.35 & -0.35 & 0.87 & 1305.85 \\ -0.71 & -0.71 & 0 & 1108.60 \\ 0 & 0 & 0 & 1 \end{bmatrix} \quad (11)$$

amongthem, $P_x = 2261.73$ $P_y = 1305.85$ $P_z = 1108.60$.

4.2. Inverse kinematics verification of robotic arm

The verification process of the inverse kinematics model is as follows: First, substitute equation (11) into the theoretical model to solve the driving parameters of each joint. Then, call the inverse solution function in the robot toolbox to calculate the same expression. The verification is completed by comparing the two sets of results.

$$\theta_1 = a\tan 2(P_y, P_x) = a\tan 2(1305.85, 2261.73) = 30^\circ \quad (12)$$

$$r = \sqrt{P_x^2 + P_y^2} = \sqrt{2261.73^2 + 1305.85^2} \approx 2611.7 \quad (13)$$

$$r' = r - 600 = 2011.7 \quad (14)$$

$$z' = P_z - 196 = -1108.60 - 196 = -1304.60 \quad (15)$$

$$d_3 = \sqrt{r'^2 + z'^2 - 2345^2} \approx 499.89 \quad (16)$$

$$\theta_2 = a\tan 2(d_3 \cdot r' - 2345 \cdot z', 2345 \cdot r' + d_3 \cdot z') = a\tan 2(1,1) = 45^\circ \quad (17)$$

The obtained verification data is θ_1=30°, θ_2=45°, and $d_3 \approx 500$, forming a closed loop, which proves the correctness of the kinematic formula. That is, it is possible to achieve trajectory programming control for the end effector of an industrial robotic arm [16].

4.3. Analysis of robotic arm workspace

Based on the parameters in Table 1, this paper utilizes MATLAB's Robotics Toolbox for kinematic simulation, successfully verifying the accuracy of the kinematic equations for the multi-joint robotic arm. Furthermore, through the Link object and SerialLink modeling function, a simulation model of the robot is established. Subsequently, a three-dimensional diagram and a top view of the intersection area between the discharge robotic arm and the carbide furnace are drawn, as shown in Figures 5 and 6, respectively[15]. As can be seen from Figures 5 and 6, the robotic arm has a wide workspace and high mobility, fully meeting the practical needs of industrial discharge operations.

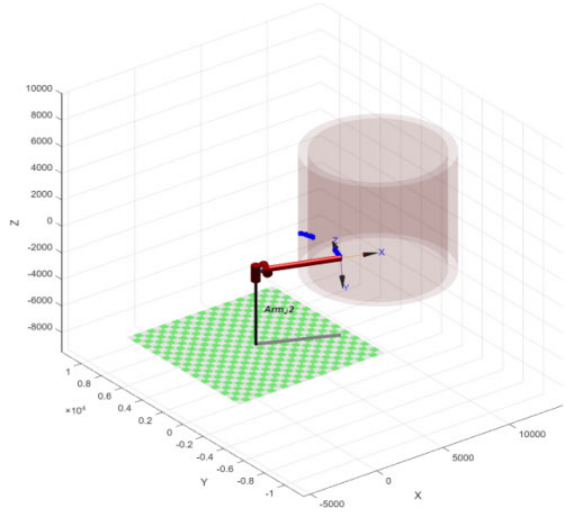


Figure 5. Spatial working range of the roboticarm

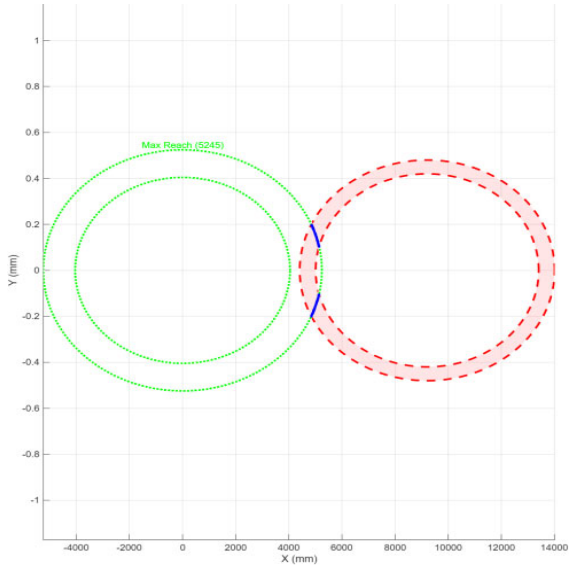


Figure 6. Top view of the spatial working range of the robotic arm

5. Space Trajectory Planning for The Discharge Robotic Arm

5.1. Planning of ablation trajectory at the mouth of carbide furnace

The designed carbide furnace mouths are categorized into trumpet-shaped mouths and cylindrical mouths based on ablation trajectories, with the appropriate mouth shape selected during production according to different operating conditions.

5.1.1. Horn-shaped furnace mouth

The mouth of the calcium carbide furnace is divided into several layers. In each layer, the burner follows a helical

ablation path from the maximum radius to the center along the contour of that layer. After ablating a circular contour, the burner repeats the action performed in the previous layer on the next layer until the wall of the calcium carbide furnace is burned through. The maximum ablation radius decreases by 1/22 after each layer is ablated. The ablation radius decreases from 250mm in the first circle to 100mm through 20 layers, and the number of ablation circles gradually decreases from 4 in the first layer to 2 in the last layer. The ablation feed distance for each layer is 30mm, ultimately forming a trumpet-shaped mouth, as shown in Figure 7.

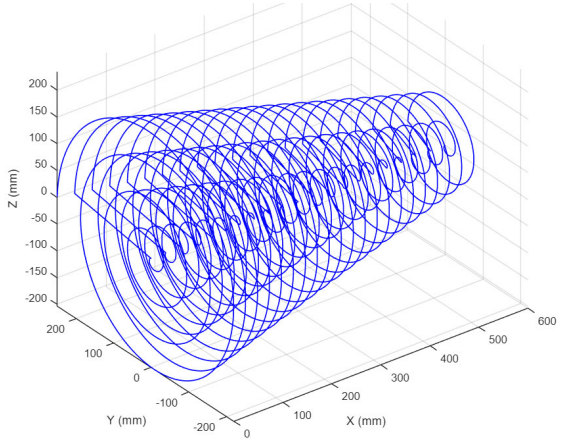


Figure 7. Ablation trajectory of bell-shaped furnace mouth

The trumpet-shaped furnace mouth is formed by burning through with the end effector of the robotic arm, and its position on the calcium carbide furnace is determined by the position of the robotic arm. The horizontal pointing height of the end effector of the robotic arm is the height of the center of the trumpet-shaped furnace mouth, as shown in Figure 8.

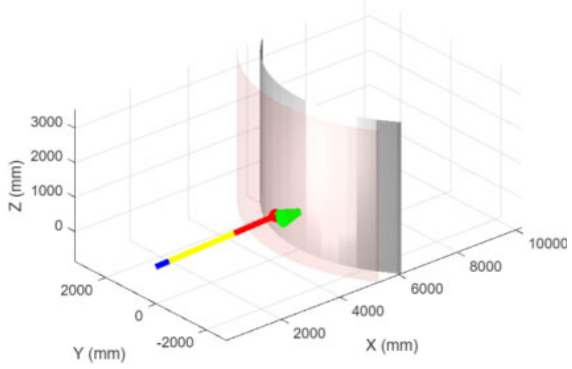


Fig. (a) Overall discharge system

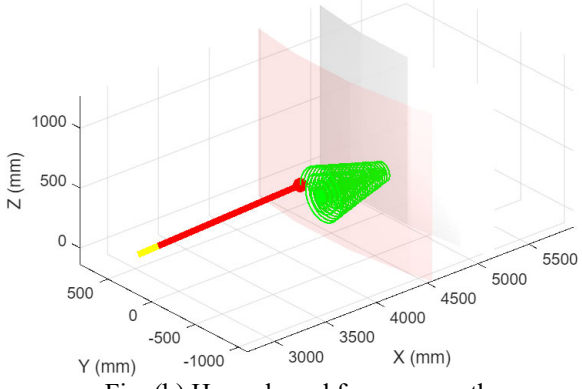


Fig. (b) Horn-shaped furnace mouth

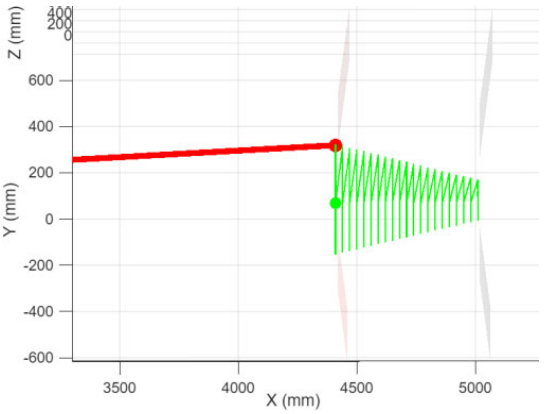


Fig. (c) Top view of furnace mouth

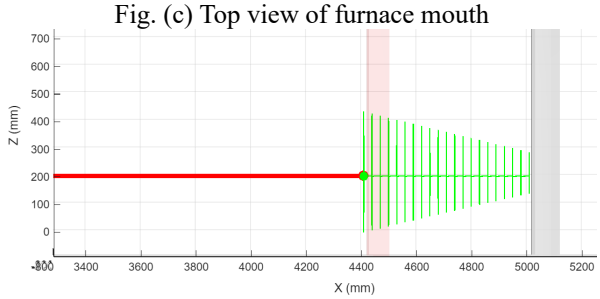


Fig. (d) Side view of furnace mouth

Figure 8. Horn-shaped furnace mouth from various perspectives

5.1.2. Cylindrical furnace mouth

The mouth of the calcium carbide furnace is divided into several layers. In each layer, the burner follows a helical ablation path from the maximum radius to the center along the contour of that layer. After ablating a circular contour, the action performed in the previous layer is repeated in the next layer until the wall of the calcium carbide furnace is burned through. The maximum ablation radius remains constant at 250mm, the number of ablation circles is constant at 4, and the ablation feed distance per layer is 30mm. Finally, a cylindrical furnace mouth is formed, as shown in Figure 9.

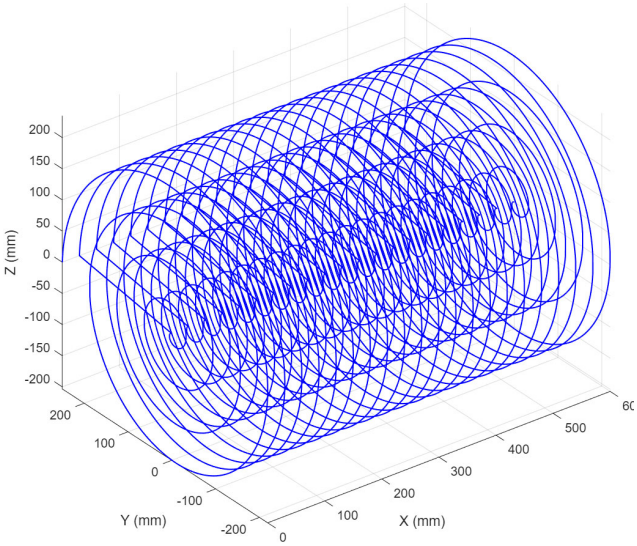


Figure 9. Ablation trajectory of cylindrical furnace mouth

The cylindrical furnace mouth is created by burning through with the end effector of the robotic arm. Its position on the calcium carbide furnace is determined by the position of the robotic arm. The horizontal pointing height of the end effector of the robotic arm corresponds to the height of the

center of the cylindrical furnace mouth, as shown in Figure 10.

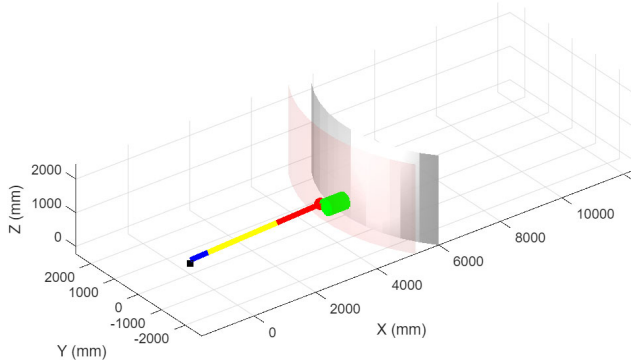


Fig. (a) Overall discharge system

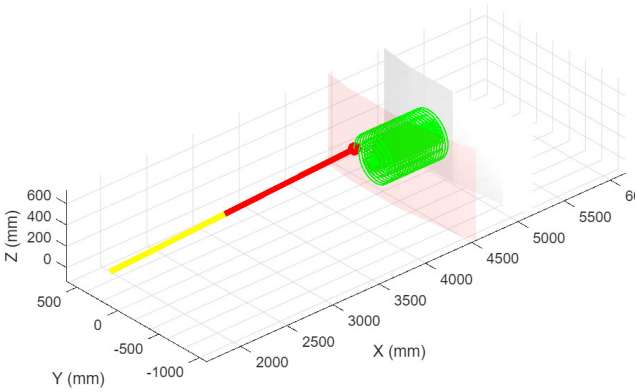


Fig. (b) Cylindrical furnace mouth

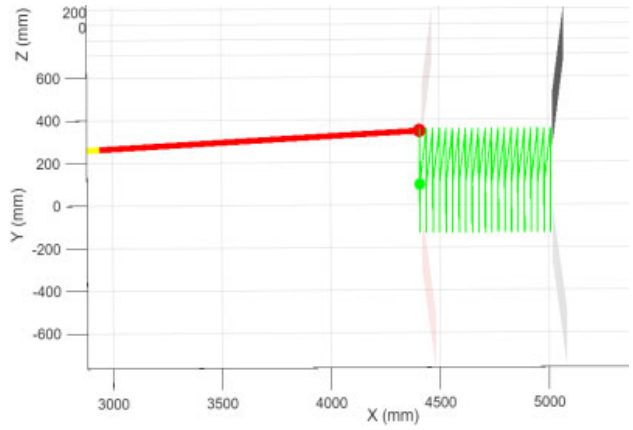


Fig. (c) Top view of furnace mouth

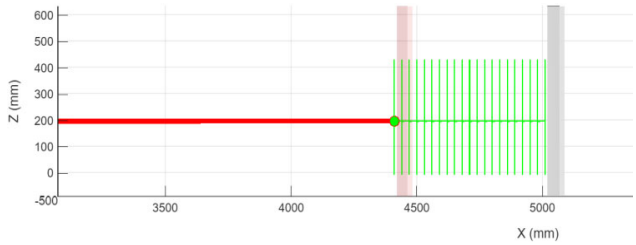


Fig. (d) Side view of furnace mouth

Figure 10. Cylindrical furnace mouth from various perspectives

5.2. Joint data simulation

In the trajectory planning phase, the joint space trajectory function jtraj (joint-space trajectory) from the Robotics Toolbox in the MATLAB platform is utilized to perform quintic polynomial interpolation on the motion process from the initial motion pose[16] to the terminal pose of the multi-joint robotic arm. The set conditions are that the velocity at both the start and end moments of the motion trajectory remains zero, and the total duration of the drilling task is set to 180 seconds. Using these settings, simulation calculations are performed synchronously for each joint, and the variation curves of the position, velocity, and acceleration of each joint during different time periods are extracted. By analyzing these curves, one can intuitively assess whether the operating state of each joint meets the requirements. Subsequently, based on the graphical results, further optimization design can be carried out. Detailed simulation results are shown in Figures 11 and 12, respectively.

Below are the variations in speed, angle, acceleration, and the length of the telescopic axis over time when the furnace mouth is trumpet-shaped, where ω1 represents the rotation axis and ω2 represents the pitch axis.

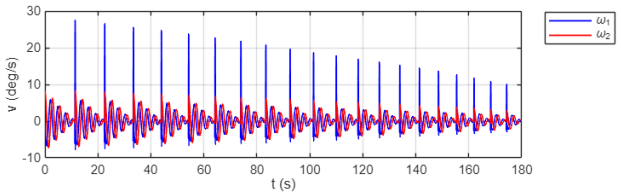


Fig. (a) Change in shaft speed over time

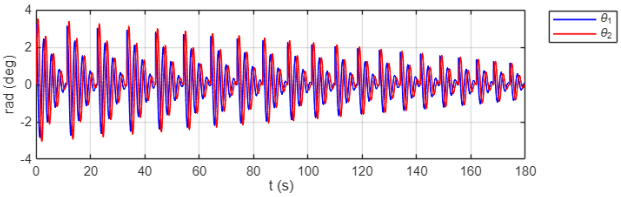


Fig.(b) Change in the angle of the axis over time

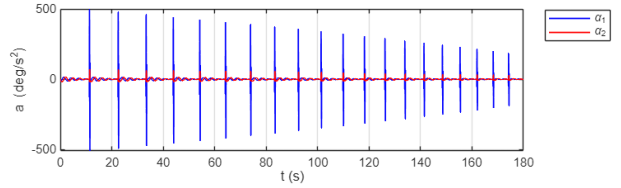


Fig.(c) Change in axial acceleration over time

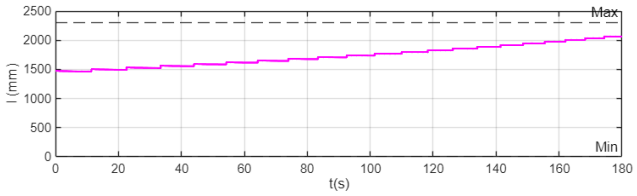


Fig.(d) Change in the length of the telescopic shaft over time

Figure 11. Data of each axis varying with time when the furnace mouth is trumpet-shaped

Below are the variations in speed, angle, acceleration, and the length of the telescopic axis with time when the furnace mouth is cylindrical, where ω_1 represents the rotation axis and ω_2 represents the pitch axis.

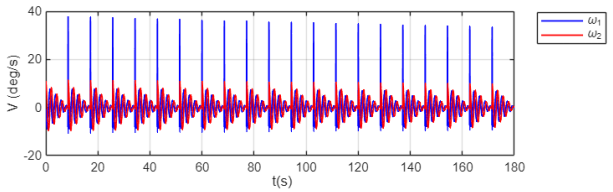


Fig. (a) Change in shaft speed over time

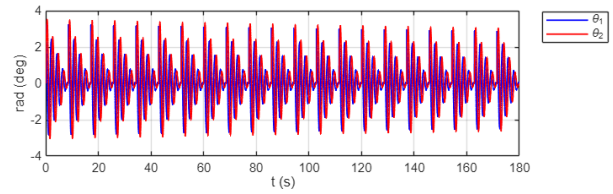


Fig.(b) Change in the angle of the axis over time

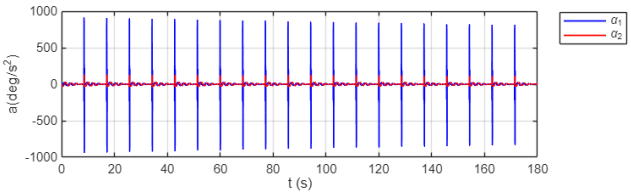


Fig.(c) Change in axial acceleration over time

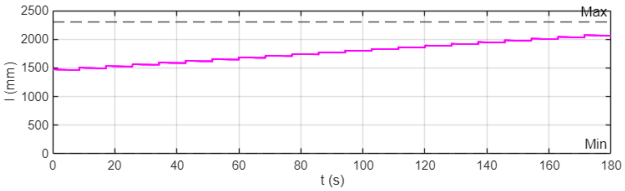


Fig.(d) Change in the length of the telescopic shaft over time

Figure 12. Data of each axis varying with time when the furnace mouth is cylindrical

From Figures 11 to 12, it can be concluded by observing the kinematic curves during the 180-second operation period that the positions, angular velocities, and angular accelerations of the three axes of the robotic arm did not experience any jumps, pauses, or singularities. Additionally, the extension and retraction of the telescopic axis maintained a smooth transition, verifying the rationality of the trajectory planning. That is, the multi-joint robotic arm with the parameters listed in Table 1 can synchronize its joints and smoothly reach the set target point in practical applications[17], with minimal vibration, meeting the requirements for discharging from a carbide furnace. According to the simulation results, compared to a cylindrical furnace mouth, a trumpet-shaped furnace mouth causes less wear to the burnthrough device, but requires more consumables for subsequent plugging than a cylindrical furnace mouth. The specific choice of furnace mouth should be determined based on different scenarios.

6. Conclusion and Outlook

The paper takes a certain company's calcium carbide furnace and its discharge robotic arm as the research object. The kinematic equations of the robotic arm are established using the D-H method, and the theoretical derivation of forward kinematics and inverse kinematics is completed. The results obtained exhibit good generality. Based on the design parameters, the kinematic equations are simulated and verified using the Robotics Toolbox in the MATLAB platform. Additionally, the workspace of the intersection area between the robotic arm and the calcium carbide furnace is analyzed. The results indicate that the designed multi-joint robotic arm has no voids or blind spots within its required workspace. For two types of calcium carbide furnace mouth structures, the motion trajectory of the burner at the end of the robotic arm from the starting point to the target point is planned, and the displacement change curves of each joint angle, angular velocity, angular acceleration, and telescopic shaft are obtained. The analysis shows that each joint moves smoothly without steps, pauses, or passing through singularities, and the telescopic amount of the telescopic shaft maintains a smooth transition, meeting the actual operational requirements. The above kinematic data can be exported in CSV format and input into a PLC (such as S7-1200) to control the hydraulic cylinder action. It plays an important role in various complex tasks, thus achieving automatic control during the actual discharge process.

References

[1] Gong, Y., Li, B., Li, D., et al. (2021). Method for constructing a power equipment fault knowledge base based on knowledge graph. Reliability and Environmental Testing of Electronic Products, 39(4), 72–77.

[2] Zhang, L., Yao, J., Yang, Y., et al. (2024). Obstacle avoidance path planning for power operation and maintenance robots based on PRRT algorithm. Journal of Mechanics and Electronics, 42(11), 58–63.

[3] Zhang, F., Huo, P., & He, Y. (2024). Structural design and path planning of mobile welding robot. Machine Tool & Hydraulic, 52(9), 36–43.

[4] Wang, H., Huang, J., Lin, W., et al. (2025). Design of PLC-based control system for ferrosilicon furnace discharge robot. Machine Tool & Hydraulic, 53(15), 104–109.

[5] Dong, J. (2024). Research on the control system of the position and orientation adjustment mechanism for a new type of ferroalloy discharge robot [Master's thesis]. Yanshan University. https://doi.org/10.27440/d.cnki.gysdu.2024.001072

[6] Ding, Q., Liu, Y., & Wang, D. (2025). Automation transformation of closed calcium carbide furnace discharge system. Polyvinyl Chloride, 53(2), 25–29.

[7] Zhang, J., Wang, J., Gu, Z., et al. (2025). Research on feed rate planning for industrial robotic blade polishing and grinding. Combination Machine Tool & Automatic Manufacturing Technology, (9), 132–137+143. https://doi.org/10.13462/j.cnki.mmtamt.2025.09.023

[8] Sun, Y. W., Jia, J. J., Xu, J. T., et al. (2022). Path, feedrate and trajectory planning for free-form surface machining: A state-of-the-art review. Chinese Journal of Aeronautics, 35(8), 12–29.

[9] Wang, L. P., Yuan, X., Si, H., et al. (2020). Feedrate scheduling method for constant peak cutting force in five-axis flank milling process. Chinese Journal of Aeronautics, 33(7), 2055–2069.

[10] Pietro, M., Geraldo, C. A. J., Luiz, E. F., et al. (1994). Combined machine for opening and closing a furnace tap hole - comprising a carriage and drive for a tapping bar or borer and a plugging unit with piston and chamber for injecting a plugging mass (German Patent No. DE4341318).

[11] Zhao, J., Zhu, X., Meng, X., et al. (2023). Application of improved whale optimization algorithm in time-optimal

trajectory planning for robotic arms. Journal of Mechanical Science and Technology, 42(3), 388–395.

[12] Wang, J., Liu, X., & Jiang, Q. (2022). Kinematic analysis and simulation of mobile mechanisms in material handling machinery. Internal Combustion Engines and Components, (07), 62–64.

[13] Yan, C. (2023, October 10). Kinematics modeling analysis of industrial robot manipulator. Integrated Circuit Application.

[14] Liu, K., & Liu, Y. (2024, June 10). Structural design and kinematic analysis of a four-joint robot. Automation Applications.

[15] Yang, W., & Gao, W. (2024, April 25). Research on the motion analysis of six-degree-of-freedom industrial robots. Information Technology and Informatization.

[16] Jiang, D., Cai, Z., Liu, Z., et al. (2022). Adaptive tracking control of continuous robotic manipulators based on reinforcement learning. Journal of System Simulation, 34(10), 2264–2271.

[17] Li, X. H., Lv, L., Sheng, R., et al. (2018). An effective construction method of modular manipulator 3D virtual simulation platform. 3D Research, 9(2), 24.